

*Faculty of Engineering*  
*Faculty of Engineering - Papers*

---

*University of Wollongong*

*Year 2004*

---

Tungsten Disulfide Nanotubes for  
Lithium Storage

G. X. Wang\*      S. Bewlay†      J. Yao‡  
H. K. Liu\*\*      S. X. Dou††

\*University of Wollongong, gwang@uow.edu.au

†University of Wollongong

‡University of Wollongong, jyao@uow.edu.au

\*\*University of Wollongong, hua@uow.edu.au

††University of Wollongong, shi@uow.edu.au

This article was originally published as Wang, GX, Bewlay, S, Yao, J et al, Tungsten Disulfide Nanotubes for Lithium Storage, *Electrochemical and Solid-State Letters*, 7(10), 2004, A321-A323. Copyright The Electrochemical Society. Original journal available <a href="http://ecsd.org/ESL/" >here</a>.

This paper is posted at Research Online.

<http://ro.uow.edu.au/engpapers/138>



## Tungsten Disulfide Nanotubes for Lithium Storage

G. X. Wang,<sup>z</sup> Steve Bewlay, Jane Yao, H. K. Liu, and S. X. Dou

Institute for Superconducting and Electronic Materials, University of Wollongong,  
New South Wales 2522, Australia

WS<sub>2</sub> nanotubes were synthesized by sintering amorphous WS<sub>3</sub> at high temperature under flowing hydrogen. High-resolution transmission electron microscopy observation revealed that the as-prepared WS<sub>2</sub> nanotubes have an open end with an inner hollow core of about 4.6 nm. We studied the lithium intercalation behavior of WS<sub>2</sub> nanotubes. The WS<sub>2</sub> nanotubes demonstrated a stable cyclability in a wide voltage range (0.1-3.1 V vs. Li/Li<sup>+</sup>). The nanotubes could provide a new class of electrode materials for lithium-ion batteries.

© 2004 The Electrochemical Society. [DOI: 10.1149/1.1788591] All rights reserved.

Manuscript submitted January 30, 2004; revised manuscript received March 13, 2004. Available electronically September 7, 2004.

Since the discovery of WS<sub>2</sub> and MoS<sub>2</sub> nanotubes by Tenne and co-workers,<sup>1-4</sup> extensive investigations have been done on the synthesis and physical and structural characterization of metal dichalcogenide nanotubes. Tenne *et al.* synthesized WS<sub>2</sub> nanotubes by treating tungsten films in an atmosphere of hydrogen sulfide and fullerene-like MoS<sub>2</sub> nanotubes by gas-phase reaction between MoO<sub>3</sub> thin-films and H<sub>2</sub>S at high temperature.<sup>1,4</sup> Rao *et al.* employed hydrogen treatment of amorphous MoS<sub>3</sub> and WS<sub>3</sub> to produce MoS<sub>2</sub> and WS<sub>2</sub> nanotubes with a high rate of yield.<sup>5</sup> These nanotubes have an average outer diameter of about 25 nm. MoS<sub>2</sub> and WS<sub>2</sub> nanotubes have also been synthesized by chemical transportation using iodine as the transport agent,<sup>6-8</sup> by the activation method (acid treatment following by sonication),<sup>9</sup> and by template synthesis.<sup>10</sup> The yield of nanotubes usually is in the range of 15-20% by these approaches. Numerous new transition metal disulfide nanotubes such as TiS<sub>2</sub>, NbS<sub>2</sub>, and TaS<sub>2</sub> have also been prepared.<sup>11,12</sup>

The one-dimensional (1D) nanotube materials have various potential applications ranging from quantum computers to nanoscale biomedical sensors.<sup>13,14</sup> Carbon nanotubes have been proposed for hydrogen storage<sup>15</sup> and for applications related to lithium-ion batteries and fuel cells.<sup>16</sup> Thin films of fullerene-like MoS<sub>2</sub> nanoparticles have ultralow friction and wear.<sup>17</sup> It has been reported that MoS<sub>2</sub> nanotubes have a moderate hydrogen storage capacity<sup>18</sup> and MoS<sub>2-x</sub>I<sub>y</sub> nanotubes have demonstrated a reversible lithium intercalation capacity of 385 mAh/g.<sup>19</sup> Lithium-ion batteries are the most advanced power sources for modern portable electronic devices. The development of next generation lithium-ion batteries with high energy relies on new electrode materials.<sup>20</sup> Here we report, for the first time, the lithium intercalation properties of WS<sub>2</sub> nanotubes in lithium-ion cells.

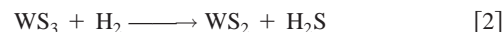
### Experimental

WS<sub>2</sub> nanotubes were synthesized by high-temperature treatment of amorphous WS<sub>3</sub> in hydrogen. Amorphous WS<sub>3</sub> was obtained by decomposition of (NH<sub>4</sub>)<sub>2</sub>WS<sub>4</sub> at low temperature under flowing argon. The starting (NH<sub>4</sub>)<sub>2</sub>WS<sub>4</sub> powders were purchased from Sigma-Aldrich Chemical. The yield of WS<sub>2</sub> nanotubes is high, more than 80%. The as-prepared WS<sub>2</sub> nanotubes were studied using 300 kV JEOL JEM-3000F transmission electron microscope (TEM) with field emission. The electrochemical properties of WS<sub>2</sub> nanotubes were measured via coin cell testing. The WS<sub>2</sub> nanotube electrodes were made by dispersing 84 wt % active materials, 8 wt % carbon black, and 8 wt % polyvinylidene fluoride (PVDF) binder in dimethyl phthalate solvent to form a homogeneous slurry. The slurry was then spread on a copper foil. The coated electrodes were dried in a vacuum oven at 120°C for 12 h and then pressed to enhance the contact between the active materials and the conductive carbons. The CR2032 coin cells were assembled in an argon-filled glove box

(Mbraun, Unilab, Germany) using lithium metal foil as the counter electrode. The electrolyte was 1 M LiPF<sub>6</sub> in a mixture of ethylene carbonate (EC) and dimethyl carbonate (DMC) (1:1 by volume, provided by Merck KgaA, Germany). The cells were galvanostatically discharged and charged in the voltage range of 0.01-3 V. Cyclic voltammetry (CV) measurements were performed on WS<sub>2</sub> nanotube electrodes using an EG&G scanning potentiostat (model 362) at a scanning rate of 0.1 mV/s.

### Results and Discussion

Amorphous WS<sub>3</sub> powders were first synthesized by decomposing ammonium tetrathiotungstate [(NH<sub>4</sub>)<sub>2</sub>WS<sub>4</sub>] at low temperature. WS<sub>2</sub> nanotubes were then prepared by sintering the as-obtained amorphous WS<sub>3</sub> at high temperature under flowing hydrogen. The two reaction steps involved are



The yield of WS<sub>2</sub> nanotubes is high, more than 80%. X-ray diffraction (XRD) was performed on the intermediate product WS<sub>3</sub> and the final product WS<sub>2</sub>, which confirmed the amorphous nature of WS<sub>3</sub> and the hexagonal phase of WS<sub>2</sub>. The WS<sub>2</sub> nanotubes were studied using JEOL-3000F transmission electron microscope with field emission. Figure 1a shows a TEM image of the as-prepared WS<sub>2</sub> nanotubes. The nanotubes in Fig. 1a have open tips, and some of them have a nearly rectangular tip shape. This is in contrast to a previous report,<sup>5</sup> which demonstrated a closed tip. The outer diameters of these WS<sub>2</sub> tubes are about 30-40 nm with a wall thickness of 15 nm. The hollow core of the nanotubes is about 4.6 nm, which is indicated in Fig. 1a. These WS<sub>2</sub> nanotubes are also short in length (a few hundred nanometers), straight, and well dispersed. Some nest-shell nanoclusters are also presented in Fig. 1a. Figure 1b shows a more magnified TEM image of WS<sub>2</sub> nanotubes, which demonstrates that nanotubes stick together to form bundles. The

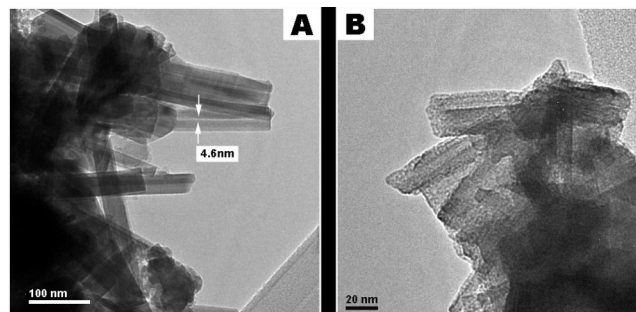


Figure 1. TEM images of WS<sub>2</sub> nanotubes.

<sup>z</sup> E-mail: gwang@uow.edu.au

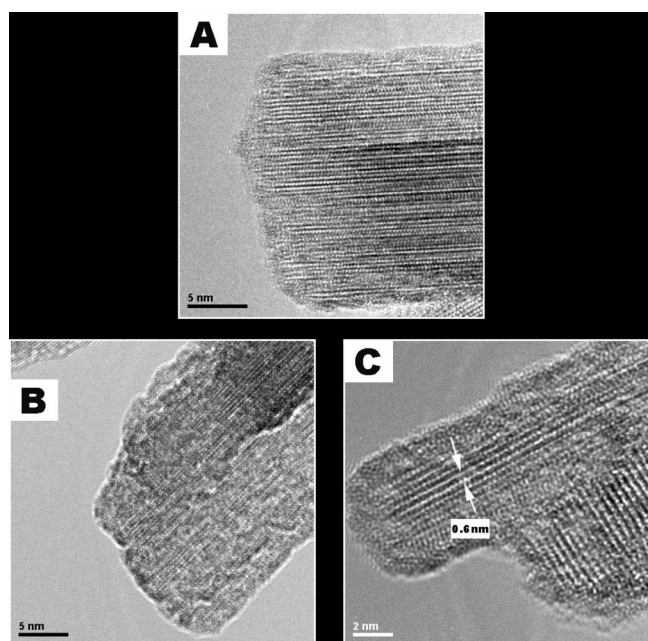


Figure 2. HRTEM images of WS<sub>2</sub> nanotubes.

outer diameter of the WS<sub>2</sub> nanotubes in Fig. 1b is about 25 nm. High-resolution TEM images of WS<sub>2</sub> nanotubes are shown in Fig. 2. Figure 2a shows the tip of a straight WS<sub>2</sub> nanotube with an outer diameter of ~20 nm. This nanotube has a nonspherical open tip and a clear-cut outside wall. Figure 2b shows the tip of another WS<sub>2</sub> nanotube, which has an onionlike cluster structure. A more magnified HRTEM image of a WS<sub>2</sub> nanotube is shown in Fig. 2c. The interlayer spacing is about 0.6 nm, corresponding to the (002) plane.

The electrochemical properties of WS<sub>2</sub> nanotubes were measured via coin cell testing. Figure 3a and b shows the cyclic voltammograms (CVs) of a WS<sub>2</sub> nanotube electrode in the first scanning cycle, the second and the third scanning cycles, respectively. In the first scanning cycle (Fig. 3a), the broad cathodic peak starts from 1.0 V and is centered at 0.5 V; whereas the anodic peak is located at 2.42 V. In the second scanning cycle, the cathodic peak at 0.5 V has disappeared, while instead, a new cathodic peak appears at 1.85 V. From the second cycle, the CV curves remain consistent and maintain a pair of redox peaks, representing the lithium intercalation plateau at ~1.85 V and the lithium deintercalation plateau at ~2.42 V.

The discharge/charge profiles of WS<sub>2</sub> nanotube electrode in the first and second cycles are presented in Fig. 4a and b. In the first cycle, the WS<sub>2</sub> nanotube electrode delivered a lithium insertion capacity of about 915 mAh/g, corresponding to 8.6 mol lithium per mole WS<sub>2</sub> nanotubes. This is much higher than for WS<sub>2</sub> powders (assuming the layered WS<sub>2</sub> host can accommodate the insertion of 1 mol Li<sup>+</sup> per mol WS<sub>2</sub><sup>21</sup>). The high lithium insertion capacity of WS<sub>2</sub> nanotubes could be ascribed to their 1D structure. The HRTEM analysis has identified that WS<sub>2</sub> nanotubes have open ends and a hollow core of about 4.6 nm in diameter. The individual straight WS<sub>2</sub> nanotubes stick together to form bundles. Some WS<sub>2</sub> nanoclusters are also present. Therefore, there are four possibilities for lithium intercalation in the WS<sub>2</sub> nanotube electrode, (i) lithium ions intercalate into intratubular sites (the hollow core) through the open end, (ii) lithium ions intercalate into intertubular sites (the sites between individual nanotubes) through diffusion in the bundles, (iii) lithium ions intercalate into WS<sub>2</sub> nano clusters and (iv) lithium ions intercalate into layered WS<sub>2</sub> structures, including in

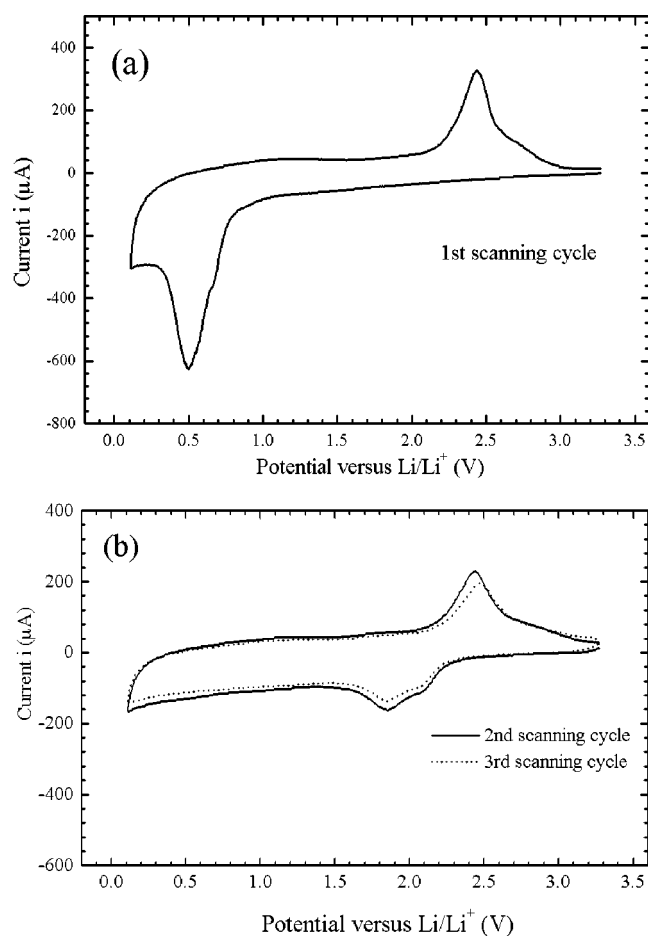
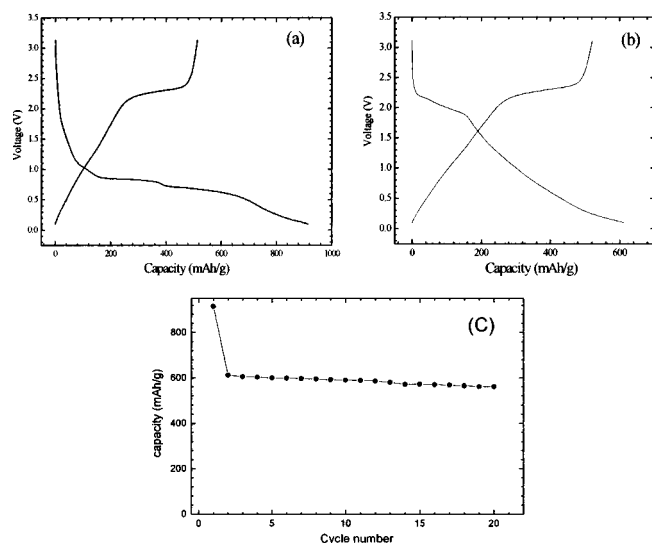


Figure 3. CVs of WS<sub>2</sub> nanotube electrode. (a) The first scanning cycle and (b) the second and the third scanning cycles.

nanotube structures and nanocluster structures. All these four possibilities may contribute to the high lithium insertion capacity of WS<sub>2</sub> nanotube electrodes.

We observed two lithium insertion plateaus at ~0.8 and ~0.6 V as well as a slope starting from 0.5 V down to the cutoff voltage of 0.1 V in the first cycle. Dominko *et al.*<sup>19</sup> attributed the 0.8 V insertion plateau to the reaction between Li<sup>+</sup> and interstitial iodine in MoS<sub>2-x</sub>I<sub>y</sub> nanotubes and the 0.6 V plateau to lithium insertion in MoS<sub>2-x</sub>I<sub>y</sub> bundles. Because our WS<sub>2</sub> nanotube sample does not contain iodine, we attribute both plateaus to lithium insertion in the WS<sub>2</sub> nanotube bundles (either intertubular or intratubular sites). Surprisingly, we found that the lithium extraction potential is located at a much higher voltage of 2.3 V vs. Li/Li<sup>+</sup>. From the second cycle, the discharge plateau is located at 2.0 V. (The discharge plateau at low potential observed in the first cycle disappeared.) The charge/discharge plateaus match very well with the anodic and cathodic peaks in the CV curves (Fig. 3). The significant difference between the first discharge and second discharge may be associated with the physical and structural changes after lithium intercalation into WS<sub>2</sub> nanotubes.

The electrochemical behavior of WS<sub>2</sub> nanotube is significantly different from that of crystalline WS<sub>2</sub> powders, which was described in a previous report.<sup>22</sup> The lithium insertion capacity was only 0.6 mol Li<sup>+</sup> per mole crystalline WS<sub>2</sub>. We attribute this difference to the 1D topology of WS<sub>2</sub> nanotubes. The 1D WS<sub>2</sub> nanotubes have an open structure. We suggest that, in the first lithiation process, lithium ions predominantly intercalate into intratubular and intertubular sites in WS<sub>2</sub> nanotubes. Once these intra- and intertubular sites are satu-



**Figure 4.** (a) Discharge/charge profiles of WS<sub>2</sub> nanotube electrode in the first cycle. (b) Discharge/charge profiles of WS<sub>2</sub> nanotube electrode in the second cycle. (c) Discharge capacity vs. cycle number for WS<sub>2</sub> nanotube electrode.

rated with Li<sup>+</sup>, lithium ions will then diffuse into WS<sub>2</sub> structure to form Li<sub>x</sub>WS<sub>2</sub> intercalation compounds due to the high concentration of Li<sup>+</sup> in these sites. During charging, a fraction of Li<sup>+</sup> ions first deintercalate from the bundles of WS<sub>2</sub> nanotubes at low potentials (observed as the slope in the charging curve), and then deintercalate from Li<sub>x</sub>WS<sub>2</sub> structures at high potentials (observed as the plateau on the charging curve). But the fraction of Li<sup>+</sup> ions trapped in the intra- and intertubular sites induce irreversible capacity. The high irreversible capacity in the first cycle may also be caused by the decomposition of electrolyte on the surface of WS<sub>2</sub> nanotubes to form a passivation layer on the electrode. From the second cycle, lithium inserted into WS<sub>2</sub> structure at high potential and then inserted into the bundles of WS<sub>2</sub> nanotubes at low potential; vice versa for deintercalation process. So, after the first cycle, the intercalation reaction dominates the electrochemical process, which is evidenced by the plateau at 2.0 V in Fig. 4b. Compared to the charge capacity, the increased discharge capacity in Fig. 4b may be due to the use of a Li auxiliary electrode. The low cutting potential in the discharge probably causes the passivation of lithium on the electrode. It is claimed that the intercalation compound (Li<sub>x</sub>WS<sub>2</sub>) decomposed to a mixture of W and Li<sub>2</sub>S for a high degree of Li insertion ( $x > 1$ ) in crystalline WS<sub>2</sub> powders.<sup>22</sup> Because the CV measurement does not detect any decomposition reactions, this process is unlikely to occur for WS<sub>2</sub> nanotubes. Figure 4c shows the lithium insertion capacity vs. the cycle number. After the first cycle, the WS<sub>2</sub> nanotube electrode exhibited stable cycling behavior in a wide voltage range of 0.1-3.1 V vs. Li/Li<sup>+</sup>.

Because the WS<sub>2</sub> nanotubes demonstrated a high discharge plateau at 2.0 V, they can be used as cathodes with a cutoff voltage of 1.5 V vs. Li/Li<sup>+</sup>. When WS<sub>2</sub> nanotube electrodes were cycled between 1.5 and 3.0 V from the second cycle, they had an approximate capacity of 200 mAh/g. Compared to the other high potential cathode materials such as LiCoO<sub>2</sub> (3.6 V), the energy density of WS<sub>2</sub> nanotubes is relatively lower. Whereas WS<sub>2</sub> nanotubes also demonstrated an interesting electrochemical behavior when cycled at low potential range. One WS<sub>2</sub> nanotube electrode was cycled between 0.1 and 1.5 V, and it showed a capacity of about 350 mAh/g.

## Conclusion

We have synthesized and characterized WS<sub>2</sub> nanotubes. The WS<sub>2</sub> nanotubes demonstrated a significant different electrochemical properties compared to the crystalline WS<sub>2</sub> powders. The WS<sub>2</sub> nanotube electrodes show stable cyclability over a wide voltage range. Nanotube materials may provide a class of versatile electrode materials for lithium-ion batteries with improved electrochemical characteristics.

## Acknowledgment

This work was supported by the Australian Research Council (ARC) through the Linkage Project "Nano anode materials for lithium-ion batteries" with industry partner Sons of Gwalia Limited.

*The University of Wollongong assisted in meeting the publication costs of this article.*

## References

1. R. Tenne, L. Margulis, M. Genut, and G. Hodes, *Nature (London)*, **360**, 444 (1992).
2. Y. Feldman, E. Wasserman, D. J. Srolowitz, and R. Tenne, *Science*, **267**, 222 (1995).
3. R. Tenne, *Adv. Mater. (Weinheim, Ger.)*, **7**, 965 (1995).
4. M. Hershinkel, L. A. Gheber, V. Volterra, J. L. Hutchison, L. Margulis, and R. Tenne, *J. Am. Chem. Soc.*, **116**, 1914 (1994).
5. M. Nath, A. Govindaraj, and C. N. R. Rao, *Adv. Mater. (Weinheim, Ger.)*, **13**, 283 (2001).
6. M. Remskar, A. Mrzel, Z. Skraba, A. Jesih, M. Ceh, J. Demsar, P. Stadelmann, F. Levy, and D. Mihailovic, *Science*, **292**, 479 (2001).
7. M. Remskar, Z. Skraba, M. Regula, C. Ballif, R. Sanjines, and Francis Levy, *Adv. Mater. (Weinheim, Ger.)*, **10**, 246 (1998).
8. M. Remskar, Z. Skraba, R. Sanjines, and F. Levy, *Appl. Phys. Lett.*, **74**, 3633 (1999).
9. E. B. Mackie, D. H. Galvan, E. Adem, S. Talapata, G. L. Yang, and A. D. Migone, *Adv. Mater. (Weinheim, Ger.)*, **12**, 495 (2000).
10. C. M. Zelenski and P. K. Dorhout, *J. Am. Chem. Soc.*, **120**, 734 (1998).
11. J. Chen, Z. L. Tan, and S. L. Li, *Angew. Chem., Int. Ed. Engl.*, **42**, 2147 (2003).
12. M. Nath and C. N. R. Rao, *J. Am. Chem. Soc.*, **123**, 4841 (2001).
13. Y. Golan, *Adv. Mater. (Weinheim, Ger.)*, **11**, 743 (1999).
14. M. Chhowalla and G. A. J. Amaratunga, *Nature (London)*, **407**, 164 (2000).
15. A. C. Dillon, K. M. Jones, T. A. Bekkedahl, C. H. Kiang, D. S. Bethune, and M. J. Heben, *Nature (London)*, **386**, 377 (1997).
16. G. Che, B. B. Lakshmi, Ellen R. Fisher, and C. R. Martin, *Nature (London)*, **393**, 346 (1998).
17. M. Chhowalla and G. A. J. Amaratunga, *Nature (London)*, **407**, 164 (2000).
18. J. Chen, N. Kuriyama, H. Yuan, H. T. Takeshita, and T. Sakai, *J. Am. Chem. Soc.*, **123**, 11813 (2001).
19. R. Dominko, D. Arcon, A. Mrzel, A. Zorko, P. Cevc, P. Venturini, M. Gaberscek, M. Remskar, and D. Mihailovic, *Adv. Mater. (Weinheim, Ger.)*, **14**, 1531 (2002).
20. J.-M. Tarascon and M. Armand, *Nature (London)*, **414**, 359 (2001).
21. M. S. Whittingham, *Science*, **192**, 1226 (1976).
22. C. M. Julien, *Mater. Sci. Eng., R.*, **40**, 47 (2003).